Magnetic instability and oxygen deficiency in Na-doped $TbMnO_3$

C. C. Yang,[1,2] M. K. Chung,[1] W.-H. Li,[1,2,*] T. S. Chan,[3] R. S. Liu,[3] Y. H. Lien,[4] C. Y. Huang,[4] Y. Y. Chan,[2] Y. D. Yao,[2] and J. W. Lynn[5]

[1]*Department of Physics, National Central University, Chung-Li 32054, Taiwan*

[2]*Institute of Physics, Academia Sinica, Taipei 11529, Taiwan*

[3]*Department of Chemistry and Center for Nano Storage Research, National Taiwan University, Taipei 106, Taiwan*

[4]*Institute of Materials Manufacturing, Chinese Culture University, Taipei 111, Taiwan*

[5]*NIST Center for Neutron Research, National Institute of Standards and Technology, Gaithersburg, Maryland 20899, USA*

(Received 22 February 2006; revised manuscript received 22 May 2006; published 11 September 2006)

Oxygen vacancies in $TbMnO_3$ were created by monovalent Na^+ doping. The effects of the interruption of the superexchange paths on the spin orderings were investigated. Chemical doping resulted in a much higher ordering temperature, which is probably associated with enhanced Tb-Tb coupling because of a reduction in Tb-Tb interatomic distances. The oxygen vacancies turned the modulated Mn spin structure into a simple commensurate one, presumably due to interruptions of the in-plane (Mn-O)–(O-Mn) superexchange paths, which reduced the significance of the next nearest-neighbor interactions of the Mn ions. The modulated spin structure of the Mn moments was found to reappear in systems with high Na doping, indicating that the anisotropic magnetic couplings had reemerged.

DOI: 10.1103/PhysRevB.74.094409 PACS number(s): 75.25.+z, 75.30.Kz, 61.12.−q, 61.10.−i

Sinusoidal antiferromagnetic ordering, with incommensurate magnetic modulation, is one of the characteristics of multiferroics $RMnO_3$, where R is a small rare-earth ion, such as Tb or Ho.[1–4] For $TbMnO_3$, the incommensurate magnetic structure of the Mn^{3+} moments has been identified,[5–10] which may be characterized by a modulation vector $(0, q_m, 0)$ that propagates along the second longest crystallographic direction b. q_m is incommensurate at the ordering temperature T_N (~42 K). It gradually decreases with decreasing temperature, and stabilizes at a transition T_{ME} (~30 K) where a new magnetic order parameter develops simultaneously with ferroelectric order.[11] The ferroelectric polarization was found[1] to develop with the polarization vector points along the longest crystallographic direction c below T_{ME}, and its direction can be reversed by the application of a magnetic field of a few Tesla, demonstrating that there exists a strong coupling between the magnetic and electric polarizations, which is not frequently found among the multiferroics.[12] Recently, the development of ferroelectricity in $TbMnO_3$ has been connected to the breaking of magnetic inversion symmetry, rather than to the formation of an incommensurate magnetic structure.[10,13]

The appearance of a modulated magnetic structure in such materials is currently explained[14] by the emergence of spin frustration that results from the competition between the ferromagnetic (FM) nearest-neighbor (NN) and antiferromagnetic (AFM) next-nearest-neighbor (NNN) Mn^{3+} superexchange (SE) spin interactions, caused by the occurrence of a significant $GdFeO_3$-type distortion and staggered $d_{3x^2-r^2}/d_{3y^2-r^2}$-type orbital ordering. The $GdFeO_3$-type distortion is a cooperative rotation of the MnO_6 octahedra, which may be characterized by a decrease in the in-plane Mn-O-Mn bond angle. Generally speaking, the distortion is enhanced when smaller ions are incorporated onto the rare-earth sites. This then results in an increase in the difference in the NNN Mn-Mn SE interaction, via the (Mn-O)–(O-Mn) path, along the two in-plane crystallographic directions.[14] Obviously, the O-O separation and the O deficiency are the two main factors that can effectively affect the interaction path. In this paper, we examine how interruptions of the in-plane (Mn-O)–(O-Mn) SE paths, by Na doping, affect the magnetic structures of the Mn and Tb ions in $TbMnO_3$,where monovalent Na^+ ions were used to create oxygen vacancies and to alter the O-O separation.

Seven polycrystalline $Tb_{1-x}Na_xMnO_{3-y}$ samples, with $x=0$–0.3 at intervals of 0.05, were prepared by the standard solid-state reaction technique. The highest doping level obtainable for the present series is $x=0.3$. Complete structural analyses of the samples were made using neutron powder-diffraction. The high-resolution neutron powder-diffraction patterns were collected on the BT-1 powder diffractometer at the NIST Center for Neutron Research, employing a Cu(311) monochromator crystal and 15′-20′-7′ FWHM angular collimations. These diffraction patterns were analyzed using the GSAS program.[15] All of the patterns could be described very well using the orthorhombic symmetry with the space group *Pbnm*.[6] A representative pattern is plotted in Fig. 1, showing the observed (crosses) and fitted (solid lines) patterns of the $x=0.15$ compound taken at 300 K, with their differences plotted at the bottom indicating they agree very well ($R_p=5.39\%$, $R_{wp}=7.31\%$, $\chi^2=1.74$). Refinements that allowed Na to enter the Mn sites gave an unacceptable occupancy factor for Na. A poorer fit ($R_p=5.76\%$, $R_{wp}=7.73\%$, $\chi^2=1.936$) resulted when we assumed that O sits were fully occupied. The refined structural parameters are listed in Table I, and the chemical formula that we obtained from the fit was $Tb_{0.851}Na_{0.149}MnO_{2.852}$ for this compound. No traces of impurity phases such as MnO, MnO_2, and Mn_2O_3 were found. We estimated the impurity phases in the samples to be less than 1%.

Analysis of the occupancy factors shows that the Na contents agree well with the stoichiometric ones, while both the in-plane and axial O are noticeably deficient (except for the $x=0$ compound) and the degree of O deficiency increases with respect to increasing x. Bond valence calculations,[16] based on the refined bond lengths, show that the Mn ions in

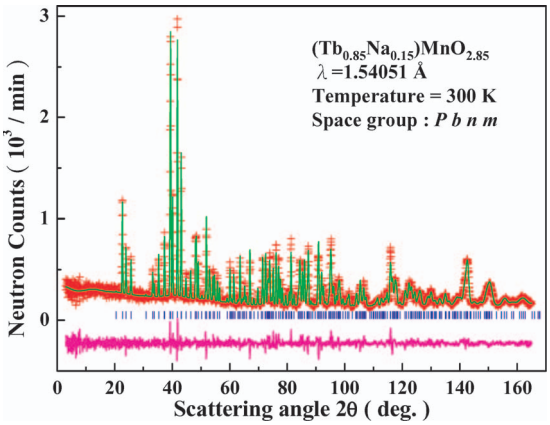

FIG. 1. (Color online) Observed (crosses) and fitted (solid lines) high-resolution neutron powder-diffraction patterns of the $x=0.15$ sample, collected at 300 K. The solid vertical lines shown below the pattern mark the calculated positions of Bragg reflections for the proposed structure.

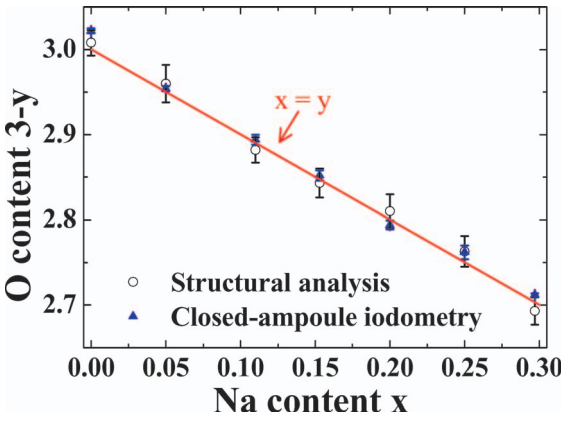

FIG. 2. (Color online) Plot of the variations of the O content with the Na content for the series of compounds, obtained from the structural analysis (open circles) and from the closed-ampoule iodometry valence determination (filled triangles). The solid line marks the curve for oxygen deficit equal to the Na content.

all of the samples are trivalent, which agrees well with what is indicated by the refined stoichiometric compositions. Similar results were also obtained using the closed-ampoule iodometry valence determination technique,[17] and from the X-ray absorption near-edge structure (XANES) Mn *K*-edge and Mn *L*-edge studies. In addition, the XANES O *K*-edge spectra show that the oxygen ions in all of the compounds are divalent. Figure 2 shows the variations of the oxygen content with the sodium content for the series of compounds, obtained from the structural (open circles) and iodometry (filled triangles) analyses. All of the structural, closed-ampoule iodometry, and XANES studies agree with the results that the Mn ions are trivalent in all samples. Apparently, the concomitant decrease in the O content completely counter-balanced the effect of monovalent Na^+ for trivalent Tb^{3+} cation substitution, such that Mn valences remained essentially constant at 3.0 in all the sample series studied. The chemical formula for this series of compounds is thus $Tb_{1-x}Na_xMnO_{3-x}$. Similar results have also been found for the $(La,Na)MnO_{3-\delta}$ system.[18,19]

The Na doping produces another important effect on the crystalline structure, in that the MnO_6 octahedral are more distorted, becoming thinner and taller. This behavior is characterized by progressive decreases in the two basal plane lattice parameters together with an increase in the axial one, so that the cell volume becomes smaller (by ~2% from $x=0$ to $x=0.3$). It is known that the ionic radius of Na^+ is ~10% larger than that of Tb^{3+}. The reduction in cell volume upon Na doping is thus mainly due to the occurrence of oxygen deficiencies in $Tb_{1-x}Na_xMnO_{3-x}$. Clearly, the separations between the atoms have been noticeably altered by Na doping. Of these, the separations between the in-plane oxygen ions are significant in affecting the NNN interactions. Adopting the notations used by Kimura *et al.*,[14] which are reproduced in the inset to Fig. 3, the in-plane oxygen separations S_{24} [between O(2) and O(4)] and S_{13} [between O(1) and O(3)], for all the compounds in the series, are shown in Fig. 3. It appears that S_{24} is about 60% shorter than S_{13} for all samples studied in the present Na-doped series. The NNN AF SE interaction for the Mn ions along the *b*-axis direction [between Mn(1) and Mn(3)] is clearly much stronger than that along the *a*-axis direction [between Mn(2) and Mn(4)]. This large difference in the NNN interactions along the two in-plane crystallographic directions has been suggested[14] to

TABLE I. Refined structural parameters of $Tb_{0.851}Na_{0.149}MnO_{2.852}$ at 300 K, where *B* represents the isotropic temperature parameter and *M* the multiplicity.

$Tb_{0.851}Na_{0.149}MnO_{2.852}$
$T=300$ K, Space group: *Pbnm*
$a=5.29748(24)$ Å, $b=5.77762(26)$ Å, $c=7.41518(33)$ Å

Atom	*x*	*y*	*z*	B_{iso}	*M*	Fraction
Tb	−0.0165(4)	0.07802(34)	$\frac{1}{4}$	0.69(3)	4	0.851(2)
Na	−0.0165(4)	0.07802(34)	$\frac{1}{4}$	0.69(3)	4	0.149(2)
Mn	$\frac{1}{2}$	0	0	0.58(6)	4	1
O(1)	0.1033(5)	0.46686(40)	$\frac{1}{4}$	0.47(6)	4	0.936(9)
O(2)	−0.2965(4)	0.32267(31)	0.04995(25)	0.73(3)	8	0.958(4)

$\chi^2=1.74$, $R_p=5.39\%$, $R_{wp}=7.31\%$

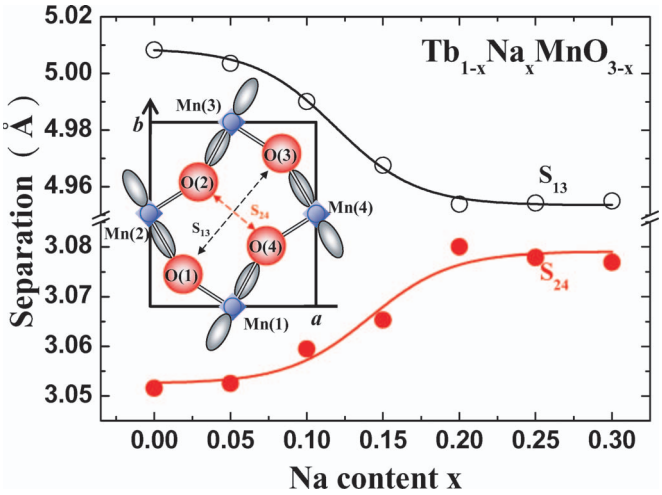

FIG. 3. (Color online) Effects of Na doping on the separations between the oxygen ions in the MnO_2 plane. It is revealed that S_{13} shortens and S_{24} correspondingly elongates in the $x<0.2$ regime, above which no noticeable change was found. The crystal structure and orbital ordering of the MnO_2 plane are shown in the inset.

be the main origin for the appearance of in-plane magnetic modulation in $TbMnO_3$. Na doping does result in a progressive increase in S_{24} and a decrease in S_{13} for x smaller than 0.2, above which no further changes were found.

It is known that the electrical conduction of $TbMnO_3$ mainly originates from the thermally activated hopping of small polarons, with an activation energy of ~62 meV. Although Na doping effectively reduces the activation energy (~40 meV for the $x=0.3$ sample), the series nevertheless remains insulating. Three transitions have been identified in $TbMnO_3$, one associated with the initial incommensurate Mn spin ordering (T_{Mn}), one with the simultaneous development of a new magnetic order parameter together with ferroelectric order (T_{ME}), and one with the quasi-long-range Tb spin ordering (T_{Tb}).[5,7] Figure 4 displays the effects of Na doping on the temperature profiles of (a) the specific heat divided by temperature (C/T) and (b) the in-phase component of the ac magnetic susceptibility (χ') of the representative samples. The peak in the specific heat that characterizes the Tb spin ordering becomes not clearly evident in the temperature range studied. The magnetic response in the susceptibility associated with the initial Mn spin ordering also becomes dramatically more pronounced and well-defined, even though the entropy changes involved in the transition are reduced in the Na-doped compounds. No obvious alterations to T_{Tb} or T_{Mn} were found when a magnetic field up to 2.5 T was applied in any of the samples. Interestingly, no definitive T_{ME} was observed in the specific heat of the doped samples.

Two types of magnetic diffraction peaks that have very different profiles were found to develop when the temperature was reduced, showing the existence of two magnetic components, each having a different origin. Figure 5 displays the high-resolution diffraction patterns taken at four characteristic temperatures. A very broad peak begins to be evident at 130 K, as can be seen in Fig. 5(c). It normalizes into two peaks [see Fig. 5(a)] at 3 K, with widths that are still much broader than the instrumental resolution function, revealing

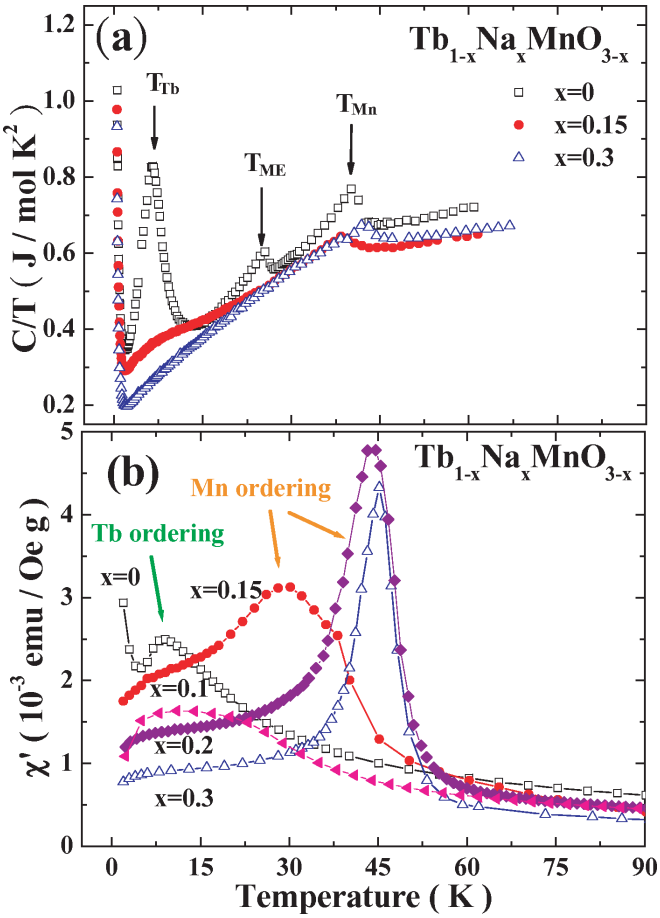

FIG. 4. (Color online) Effects of Na doping on the temperature profiles of (a) the specific heat divided by temperature C/T and (b) the in-phase component of the ac magnetic susceptibility χ', measured using a weak probing field with a rms strength of 1 Oe and a frequency of 100 Hz. Upon Na doping the peak that characterizes the Tb spin ordering becomes not evidently shown in the temperature range studied, and the magnetic responses associated with the Mn spin ordering becomes more pronounced. The upturn in the specific heat at the lowest temperature is likely due to a Schottky anomaly.

the appearance of a short-range magnetic ordering with a correlation length of $\xi \approx 55$ Å at 3 K. In addition, a resolution-limited peak, which characterizes the appearance of a long-range magnetic ordering, is also evident in the pattern taken at 3 K. High intensity neutron diffraction patterns were then taken on the BT-9 triple-axis spectrometer at National Institute of Standards and Technology (NIST), employing a pyrolytic graphite PG(002) monochromator crystal to select an incident wavelength of 2.359 Å, coarse collimations to increase the magnetic intensities, a PG filter, and a PG(002) analyzer crystal to discriminate against inelastic scattering. The short-range spin correlations persist up to quite high temperatures, as can be seen in the temperature dependence of the $\{\frac{1}{2}\frac{1}{2}\frac{1}{2}\}$ peak intensity plotted in Fig. 6, where a transition associated with long-range ordering at $T_{LR} \approx 40$ K and developments of short-range ordering at $T_{SR} \approx 140$ K are seen. Likewise, $T_{SR} \approx 75$ K and $\xi \approx 90$ Å were found for the $x=0.1$ sample at 1.4 K. This compares

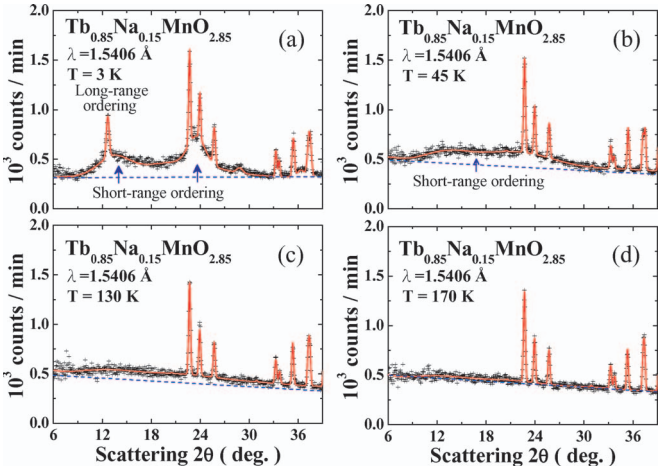

FIG. 5. (Color online) High-resolution diffraction patterns taken on the $x=0.15$ sample at four characteristic temperatures. A very broad peak begins to be evident at 130 K, which normalizes into two peaks at 3 K, with widths that are still much broader than the instrumental resolution, revealing the appearance of a short-range ordering. A resolution-limited peak, which characterizes the appearance of a long-range ordering, is also evident in the pattern taken at 3 K.

with $T_{\mathrm{Tb}} \approx 7$ K and $\xi \approx 140$ Å for the undoped compound.[7]

Two magnetic components were hence observed. The long-range and the short-range orderings were likely to be associated with two different sublattices. Long-range Mn spin ordering with $T_{\mathrm{Mn}}=46$ K and short-range Tb spin ordering with $T_{\mathrm{Tb}}=7$ K have been identified[7] in $TbMnO_3$. The long- and short-range orderings observed in the present $x=0.15$ compound can be associated, respectively, with the Mn and Tb spin orderings. The reduction in ξ due to Na doping is understandable, since the Tb ions are partially replaced by Na ions. However, the huge enhancement in T_{Tb} is surprising, and we believe it to be associated with the oxygen deficiency in the systems: Two types of magnetic couplings between the two neighboring Tb ions may be anticipated, a

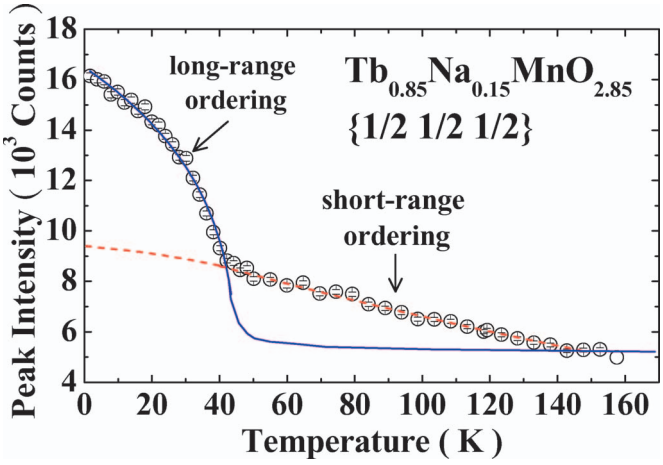

FIG. 6. (Color online) Temperature dependence of the $\{\frac{1}{2}\frac{1}{2}\frac{1}{2}\}$ peak intensity of the $x=0.15$ sample, revealing a two-step transition for the long- and short-range spin orderings, with $T_{\mathrm{LR}} \approx 40$ K and $T_{\mathrm{SR}} \approx 140$ K, respectively.

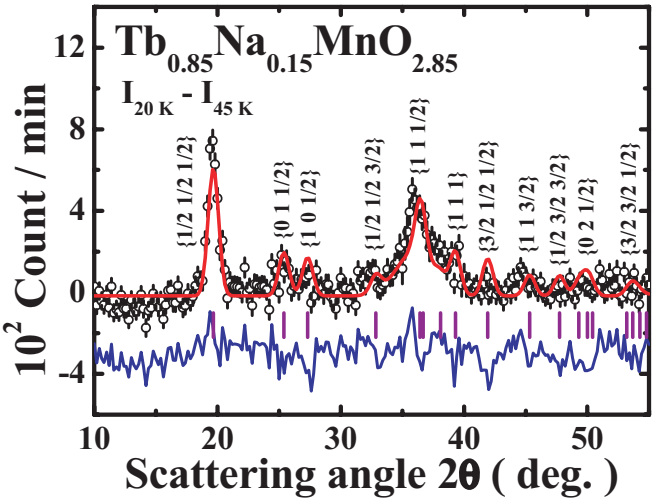

FIG. 7. (Color online) Observed (open circles) and calculated (solid curves) magnetic diffraction patterns associated with the Mn and Tb spin orderings developed from 45 to 20 K in the $x=0.15$ sample. No incommensurate magnetic modulation was seen for the Mn moments.

ferromagnetic indirect-exchange (FMIE) coupling[20] and an antiferromagnetic superexchange (AFMSE) coupling mediated through the O ion located between them. Competition between the FMIE and AFMSE couplings results in a complicated spin arrangement for the Tb ions in the undoped compound.[7] Na doping not only creates oxygen vacancies that weaken the AFMSE, but also shortens the in-plane Tb-Tb separations that enhance the FMIE. As a result, it turns to a stronger FM coupling, which could give rise to a higher T_{Tb}. Nevertheless one has to explain why the structure remains antiferromagnetic. Higher Na doping creates more oxygen vacancies and dilutes more Tb with Na, which weaken the correlations among the Tb ions. No significant Tb-Tb correlations were found in the $x=0.25$ and 0.3 samples.

The diffraction pattern that characterizes the long-range spin ordering is shown in Fig. 7. A simple diffraction pattern that represents a relatively simple commensurate magnetic structure is seen for the Mn spin in the $x=0.15$ sample. The spin arrangement for the in-plane Mn ions may be viewed as consisting of alternating ferromagnetic and antiferromagnetic chains along the [110] direction, with the spins along the c axis forming an up-up-down-down arrangement. The solid curve shown in Fig. 7 is the calculated pattern, based on the model shown in Fig. 8, with a Mn moment of $\langle \mu_Z \rangle_{\mathrm{Mn}} = 3.74(8)\mu_{\mathrm{B}}$ and a Tb moment of $\langle \mu_Z \rangle_{\mathrm{Tb}} = 0.54(11)\mu_{\mathrm{B}}$. A reasonable agreement between the observed and calculated patterns was obtained. Table II lists the directions and values of the magnetic moments for the Mn and Tb ions in the magnetic unit cell. This proposed magnetic structure was obtained on a powder sample and using data of large statistical fluctuations, and it should be considered as a tentative one. Studies using single crystal samples are needed to uncover the details of the magnetic structure. Note that the saturated Mn moment obtained for the 15% Na-doped compound is 5% smaller than the undoped compound.[6,10] The $\langle \mu_Z \rangle_{\mathrm{Tb}} = 0.54(11)\mu_{\mathrm{B}}$ indicates the moment develop on the Tb ions

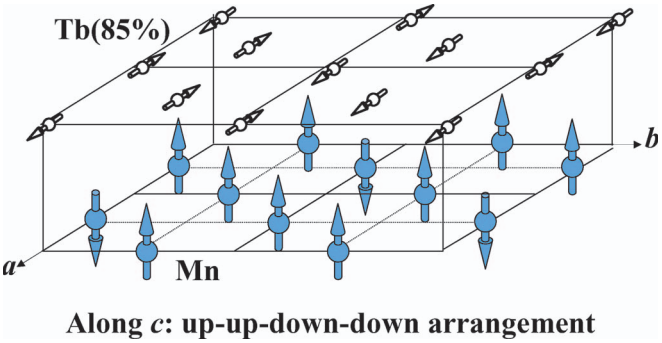

FIG. 8. (Color online) Proposed magnetic structure of the Mn and Tb ions in the $x=0.15$ sample. This spin arrangement may be viewed as consisting of alternating ferromagnetic and antiferromagnetic chains along the [110] direction.

between 20 and 45 K. Comparing the magnetic intensities obtained at 1.4 and 150 K then gives a Tb moment of $1.07(11)\mu_B$ at 1.4 K. We note that this moment obtained for the Tb ions was calculated from the short-range scattering observed at 1.4 K, at which the main fraction of the Tb moments remains only partially ordered. Similar patterns were seen for the $x=0.1$ sample. Interestingly, Na doping suppresses the magnetic modulation of the Mn spins. Surprisingly, the magnetic modulation reemerges at higher Na doping, as can be seen in Fig. 9, where the magnetic diffraction pattern of the $x=0.3$ sample taken at 18 K clearly displays a complicated spectrum, with the appearance of incommensurate satellite peaks (indicated by arrows) that may be characterized by the modulation vector (0, 0.275, 0). The temperature profiles of the modulation peaks are evidently different from those of the main reflections, as shown in Fig. 10, indicating that the modulation vector may vary with temperature. It does, however, stabilize below $T_{ME}\approx 10$ K. Similar patterns were seen for the $x=0.25$ sample.

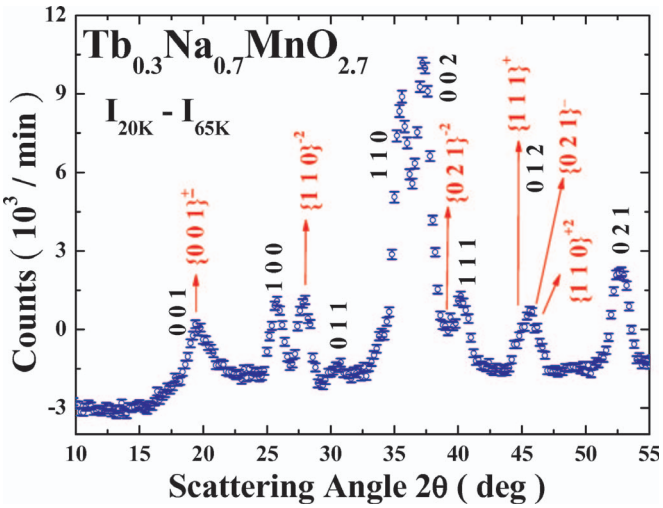

FIG. 9. (Color online) Magnetic diffraction pattern associated with the long-range spin ordering of the $x=0.3$ sample, where the arrows indicate the peaks corresponding to an incommensurate magnetic structure.

The incommensurate magnetic structure for the Mn moments in $TbMnO_3$ is currently understood[14] to be due to differences in the NNN SE interactions between the Mn ions along the two in-plane crystallographic directions, resulting

TABLE II. Directions and values of the magnetic moments for the Mn and Tb ions in the magnetic unit cell of $Tb_{0.851}Na_{0.149}MnO_{2.852}$ at 20 K. Only one block of the magnetic unit cell is shown. Magnetic moments in neighboring planes are the following $m(x,y,z+\frac{1}{4})=m(x,y,z)$ and $m(x,y,z+\frac{1}{2})=m(x,y,z+\frac{3}{4})=-m(x,y,z)$.

$Tb_{0.851}Na_{0.149}MnO_{2.852}$ at 20 K Magnetic unit cell doubles the crystalline one along all three axis directions Along the c-axis direction: up-up-down-down arrangement.						
Atom	x	y	z	m_a	m_b	m_c
Mn	$\frac{1}{4}$	0	0	0	0	3.74(8)
Mn	$\frac{3}{4}$	0	0	0	0	−3.74(8)
Mn	0	$\frac{1}{4}$	0	0	0	3.74(8)
Mn	$\frac{1}{2}$	$\frac{1}{4}$	0	0	0	3.74(8)
Mn	$\frac{1}{4}$	$\frac{1}{2}$	0	0	0	−3.74(8)
Mn	$\frac{3}{4}$	$\frac{1}{2}$	0	0	0	3.74(8)
Mn	0	$\frac{3}{4}$	0	0	0	3.74(8)
Mn	$\frac{1}{2}$	$\frac{3}{4}$	0	0	0	3.74(8)
Tb	−0.0083	0.03901	$\frac{1}{8}$	0.54(11)	0	0
Tb	0.4917	0.03901	$\frac{1}{8}$	−0.54(11)	0	0
Tb	0.2541	0.28901	$\frac{1}{8}$	−0.54(11)	0	0
Tb	0.7541	0.28901	$\frac{1}{8}$	−0.54(11)	0	0
Tb	−0.0083	0.53901	$\frac{1}{8}$	−0.54(11)	0	0
Tb	0.4917	0.53901	$\frac{1}{8}$	0.54(11)	0	0
Tb	0.2541	0.78901	$\frac{1}{8}$	0.54(11)	0	0
Tb	0.7541	0.78901	$\frac{1}{8}$	0.54(11)	0	0

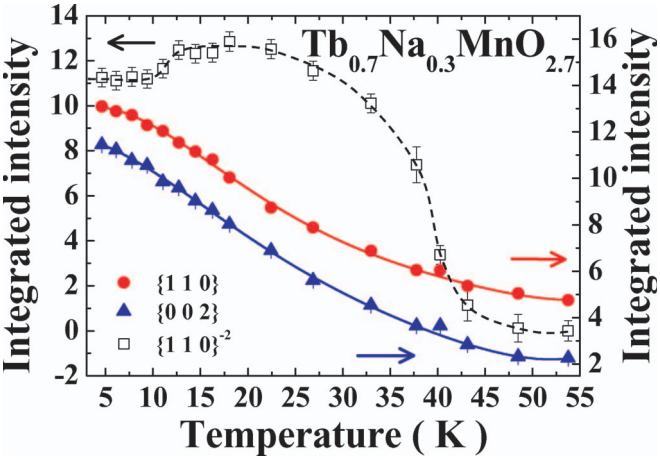

FIG. 10. (Color online) Plot of the temperature dependencies of the peak intensities of three representative reflections. Different temperature profiles for the main and the modulation peaks are clearly revealed.

from large differences in the in-plane oxygen separations S_{24} and S_{13}. The reduction in S_{13} together with the increase in S_{24}, due to Na doping (see Fig. 3), does reduce the imbalance in the NNN interactions along the two crystallographic directions. However, the maximum amount of change in S_{24} or S_{13} was only about 1%, which indicates a very delicate balance of interactions in this system. In perovskite manganites, for example, both the NN and NNN interactions between the Mn ions are mediated through the nearby oxygen ions. An oxygen shortage then definitely places significant influence on the interactions, hence the spin arrangement. In the low-x regime, where only a few oxygen vacancies have been created, the influences would mainly be on the interruption of the NNN SE interactions, such that the difference in the Mn-Mn interactions along the two crystallographic directions due to the NNN interaction becomes small. A simple commensurate structure, as the one shown in Fig. 8, may then result. With the introduction of more oxygen vacancies, the alternations in the NN interactions can become more significant. Evidently, the interactions along the two crystallographic directions can once again become significantly different, since the similarity in the atomic arrangement along the [110] direction and the $[1\bar{1}0]$ direction may be broken due to a significant lack of oxygen atoms. Magnetic modulation may then redevelop.

The ionic radius of the rare-earth ions in $R\mathrm{MnO}_3$ is known to affect the magnetic structure of the Mn moments. In this study, we show directly that oxygen content can also affect the magnetic structures of both Mn and Tb in TbMnO_3. Two magnetic components were observed in the 15% Na-doped compound at 1.4 K. A long-range one begins to develop at 40 K, and a short-range one persists up to 140 K. We suggest that the long-range ordering was associated with the Mn spins and the short-range one was originated mostly from the Tb spin correlations.

The work was supported by the National Science Council of Taiwan, the Republic of China under Grant No. NSC 94-2120-M-008-003.

*Corresponding author. Electronic address: whli@phy.ncu.edu.tw

[1] T. Kimura, T. Goto, H. Shintani, K. Ishizaka, T. Arima, and Y. Tokura, Nature (London) **426**, 55 (2003).
[2] Th. Lottermoser, Th. Lonkai, U. Amann, D. Hohlwein, J. Ihringer, and M. Fiebig, Nature (London) **430**, 541 (2004).
[3] N. Hur, S. Park, P. A. Sharma, J. S. Ahn, S. Guha, and S.-W. Cheong, Nature (London) **429**, 392 (2004).
[4] S. Kobayashi, T. Osawa, H. Kimura, Y. Noda, N. Kasahara, S. Mitsuda, and K. Kohn, J. Phys. Soc. Jpn. **73**, 1593 (2004).
[5] S. Quezel, F. Tcheou, J. Rossat-Mignod, G. Quezel, and E. Roudaut, Physica B & C **86**, 916 (1977).
[6] J. Blasco, C. Ritter, J. Garcia, J. M. de Teresa, J. Perez-Cacho, and M. R. Ibarra, Phys. Rev. B **62**, 5609 (2000).
[7] R. Kajimoto, H. Yoshizawa, H. Shintani, T. Kimura, and Y. Tokura, Phys. Rev. B **70**, 012401 (2004).
[8] Munoz, M. T. Casais, J. A. Alonso, M. J. Martinez-Lopez, J. L. Martinez, and M. T. Fernandez-Diaz, Inorg. Chem. **40**, 1020 (2001).
[9] O. P. Vajk, M. Kenzelmann, J. W. Lynn, S. B. Kim, and S. W. Cheong, Phys. Rev. Lett. **94**, 087601 (2005).
[10] M. Kenzelmann, A. B. Harris, S. Jonas, C. Broholm, J. Schefer, S. B. Kim, C. L. Zhang, S.-W. Cheong, O. P. Vajk, and J. W. Lynn, Phys. Rev. Lett. **95**, 087206 (2005).
[11] The recent extensive single crystal data on TbMnO_3 (Ref. 10) clearly demonstrate that the magnetic ordering wave vector remains incommensurate in the ferroelectric phase, rather than locking into a commensurate value as had been previously thought. We, therefore, refer to this transition, where a new magnetic order parameter develops simultaneously with ferroelectric order, as T_{ME} rather than T_{lock}. These new order parameters develop continuously, indicating that the transition is second order in nature.
[12] H. Schmid, Ferroelectrics **162**, 317 (1994).
[13] G. Lawes, A. B. Harris, T. Kimura, N. Rogado, R. J. Cava, A. Aharony, O. Entin-Wohlman, T. Yildrim, M. Kenzelmann, C. Broholm, and A. P. Ramirez, Phys. Rev. Lett. **95**, 087205(R) (2005).
[14] T. Kimura, S. Ishihara, H. Shintani, T. Arima, K. T. Takahashi, K. Ishizaka, and Y. Tokura, Phys. Rev. B **68**, 060403(R) (2003).
[15] A. C. Larson and R. B. Von Dreele, Los Alamos National Laboratory, Los Alamos, NM, Report No. LA-UR-86-748, 1990 (unpublished).
[16] N. E. Brese and M. O'Keeffe, Acta Crystallogr., Sect. B: Struct. Sci. **47**, 192 (1991).
[17] P. Karen, E. Suard, F. Fauth, and P. M. Woodward, Solid State Sci. **6**, 1195 (2004).
[18] W. H. McCarroll, Ian D. Fawcett, M. Greenblatt, and K. V. Ramanujachary, Solid State Chem. **146**, 88 (1999).
[19] R. N. Singh, C. Shivakumara, N. Y. Vasanthacharya, S. Subramanian, M. S. Hegde, H. Rajagopal, and A. Sequeira, J. Solid State Chem. **137**, 19 (1998).
[20] W. C. Koehler, H. R. Child, E. O. Wollan, and J. W. Cable, Jpn. J. Appl. Phys., Suppl. **34**, 1335 (1963).